

1 **Comparison of different linear-combination modelling algorithms for short-** 2 **TE proton spectra**

3 Helge J. Zöllner^{1,2}, Michal Považan^{1,2}, Steve C. N. Hui^{1,2}, Sofie Tapper^{1,2}, Richard A. E. Ed-
4 den^{1,2}, Georg Oeltzschner^{1,2,*}

5 ¹ *Russell H. Morgan Department of Radiology and Radiological Science, The Johns Hopkins*
6 *University School of Medicine, Baltimore, MD, United States*

7 ² *F. M. Kirby Research Center for Functional Brain Imaging, Kennedy Krieger Institute, Balti-*
8 *more, MD, United States*

9

10 ***Corresponding author:**

11 Georg Oeltzschner, Ph.D.

12 Division of Neuroradiology, Park 367G

13 The Johns Hopkins University School of Medicine

14 600 N Wolfe St

15 Baltimore, MD 21287

16 goeltzsl@jhmi.edu

17

18 *Word count: 5179*

19 *Figure count: 6*

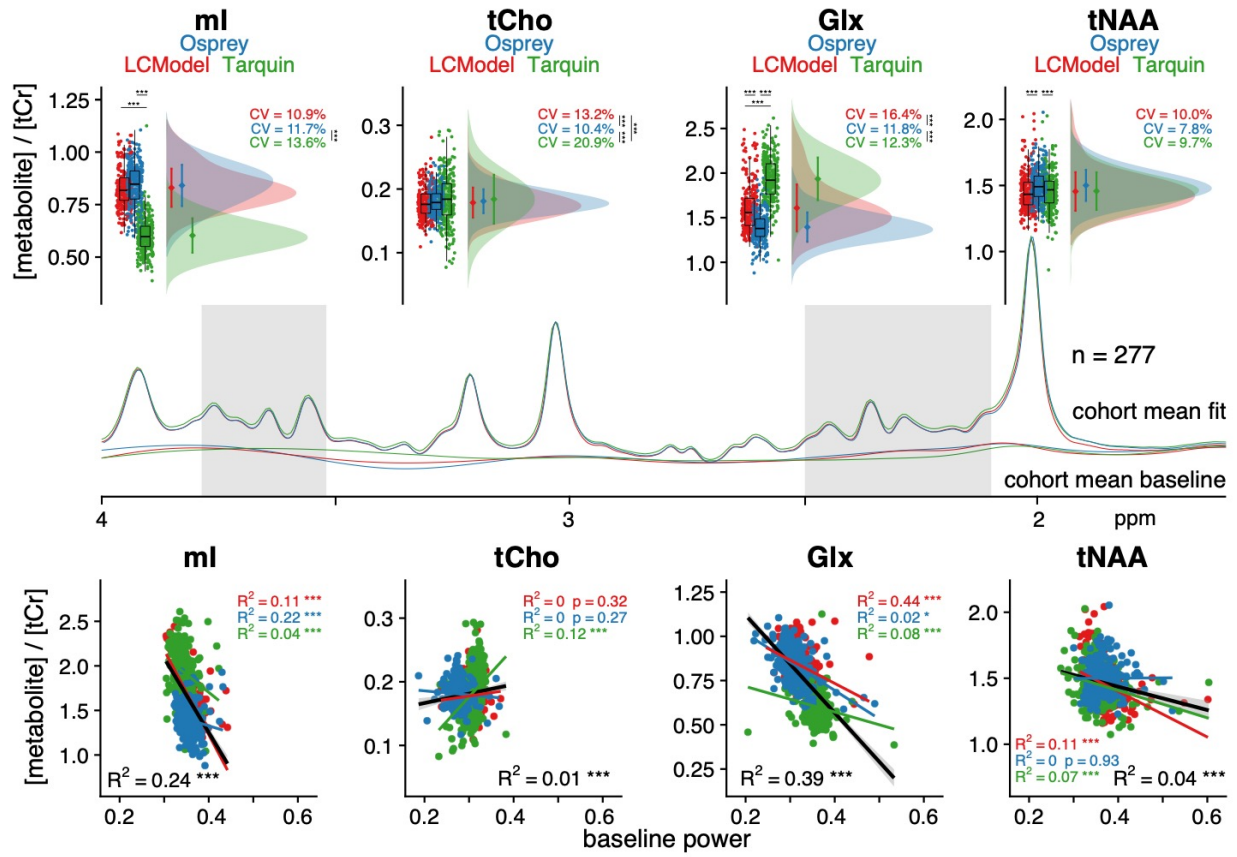
20 *Keywords: MRS, linear-combination modelling, short-echo-time spectra, LCM*

21 *Abbreviations: linear-combination modelling – LCM, total N-acetylaspartate – tNAA, total cho-*

22 *line – tCho, myo-Inositol – mI, glutamate+glutamine – Glx, total creatine – tCr, macromolecular*

23 *– MM, Hankel singular value decomposition – HSVD, coefficient of variation – CV*

24 Graphical Abstract



25

26

27 **Abstract**

28 Short-TE proton MRS is used to study metabolism in the human brain. Common analysis meth-
29 ods model the data as linear combination of metabolite basis spectra. This large-scale multi-site
30 study compares the levels of the four major metabolite complexes in short-TE spectra estimated
31 by three linear-combination modelling (LCM) algorithms.

32
33 277 medial parietal lobe short-TE PRESS spectra (TE = 35 ms) from a recent 3T multi-site study
34 were pre-processed with the Osprey software. The resulting spectra were modelled with Osprey,
35 Tarquin and LCMModel, using the same three vendor-specific basis sets (GE, Philips, and Sie-
36 mens) for each algorithm. Levels of total N-acetylaspartate (tNAA), total choline (tCho), myo-
37 inositol (mI), and glutamate+glutamine (Glx) were quantified with respect to total creatine (tCr).

38 Group means and CVs of metabolite estimates agreed well for tNAA and tCho across vendors
39 and algorithms, but substantially less so for Glx and mI, with mI systematically estimated lower
40 by Tarquin. The cohort mean correlation coefficient for all pairs of LCM algorithms across all
41 datasets and metabolites was $\overline{\mathbf{R}^2} = 0.39$, indicating generally only moderate agreement of indi-
42 vidual metabolite estimates between algorithms. There was a significant correlation between lo-
43 cal baseline amplitude and metabolite estimates (cohort mean $\overline{\mathbf{R}^2} = 0.10$).

44 While mean estimates of major metabolite complexes broadly agree between linear-combination
45 modelling algorithms at group level, correlations between algorithms are only weak-to-moderate,
46 despite standardized pre-processing, a large sample of young, healthy and cooperative subjects,
47 and high spectral quality. These findings raise concerns about the comparability of MRS studies,
48 which typically use one LCM software and much smaller sample sizes.

49 Introduction

50 Proton MRS allows in-vivo research studies of metabolism^{1,2}. Single-voxel MR spectra from the
51 human brain are frequently acquired using PRESS localization³, and can be modelled to esti-
52 mate metabolite levels. Accurate modelling is hampered by poor spectral resolution at clinical
53 field strengths, and for short-echo-time spectra, metabolite signals overlap with a broad back-
54 ground consisting of fast-decaying macromolecule and lipid signals. Linear-combination model-
55 ling (LCM) of the spectra maximizes the use of prior knowledge to constrain the model solution,
56 and is recommended by recent consensus⁴. LCM algorithms model spectra as a linear combina-
57 tion of (metabolite and macromolecular (MM)) basis functions, and typically also include terms
58 to account for smooth baseline fluctuations.

59
60 Several LCM algorithms are available to quantify MR spectra (**Table 1** describes some of the
61 most widely used: Osprey⁵, INSPECTOR⁶, Tarquin⁷, AQSES⁸, Vespa⁹, QUEST¹⁰, LCMModel¹¹).
62 The implementations (open-source vs. compiled ‘black-box’), modelling approaches (modelling
63 domain and baseline model), and their licensure practices are diverse.

64 Surprisingly few studies have compared the performance of different LCM algorithms. Cross-
65 validation of quantitative results has almost exclusively been performed in the context of bench-
66 marking new algorithms against existing solutions. In-vivo comparisons are often limited to
67 small sample sizes, whether analyzing spectra from animal models^{7,12,13} or human subjects^{7,8,12}.
68 To the best of our knowledge, two exceptions compared the LCM performance of different algo-
69 rithms in rat brain¹⁴ and human body¹⁵, respectively. Most studies report good agreement be-
70 tween results from different algorithms, inferring this from group-mean comparisons, or observ-
71 ing that differences between clinical groups are consistent regardless of the algorithm ap-
72 plied^{14,16}. Correlations of estimates from different algorithms are rarely reported; however, a high
73 correlation between LCMModel and Tarquin results was found in the rat brain at ultra-high field¹⁴.

74 Despite the fact that LCM has been used to analyze thousands of studies (**Table 1**), a compre-
75 hensive assessment of the agreement between the algorithms is lacking, and the relationship be-
76 tween the choice of model parameters and quantitative outcomes is poorly understood. To begin
77 to address this gap, we conducted a large-scale comparison of short-TE in-vivo MRS data using
78 three LCM algorithms with standardized pre-processing. While recent expert consensus recom-
79 mends using measured MM background spectra, data for different sequences are not broadly

80 available or integrated in LCM software. This manuscript investigates current common practice,
81 and therefore all models included simulated MM basis functions as defined in LCModel. We
82 compared group-mean quantification results of four major metabolite complexes from each LCM
83 algorithm, performed between-algorithm correlation analyses, and investigated local baseline
84 power and creatine modelling as potential sources of differences between the algorithms.
85

86 **Table 1.** Overview of linear-combination modelling algorithms. The domain (time TD or fre-
87 quency FD) of modelling and the baseline model approach are specified. *Citations re-
88 ported from Google Scholar on September 14, 2020.

Name	Modelling Domain, Baseline approach	Cost	Code Availability	Published	Citations*
Osprey	FD, spline baseline	free	open	2020	1
INSPECTOR	FD, 1 st -order polynomial	free	open	2018	0
Tarquin	TD, smooth baseline	free	open	2011	259
AQSES (jMRUI)	TD, spline baseline	free	closed	2007	141
Vespa	FD, wavelet baseline	free	open	2006	72
QUEST (jMRUI)	TD, spline baseline	free	closed	2004	34
LCModel	FD, spline baseline	\$13,300	closed	1992	3482

89

90 Methods

91 Participants & acquisition

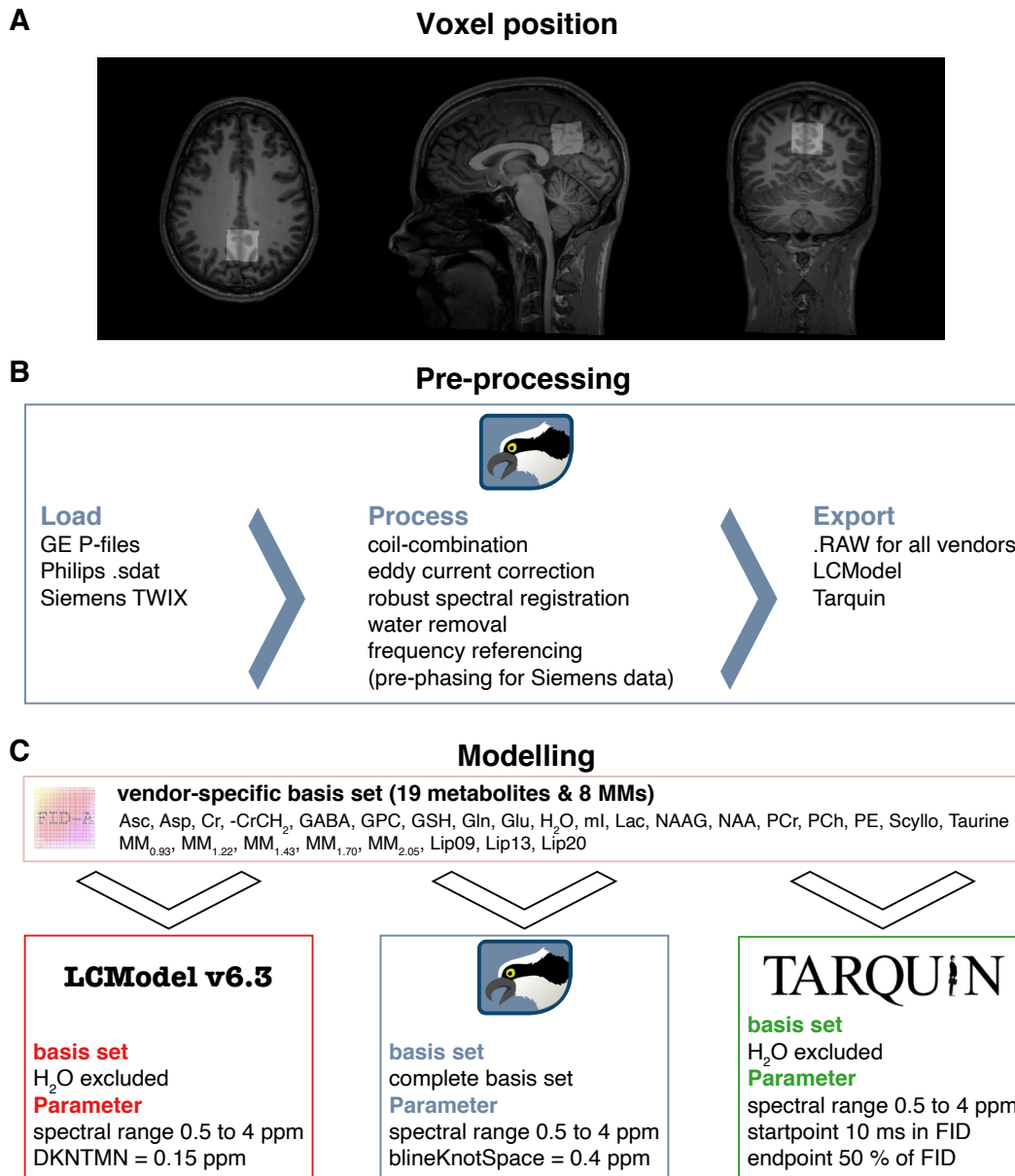
92 277 single-voxel short-TE PRESS brain datasets from healthy volunteers acquired in a recent 3T
93 multisite-study¹⁷ were included in this analysis. Data were acquired at 25 sites (with up to 12
94 subjects per site) on scanners from three different vendors (GE: 8 sites with n = 91; Philips: 10
95 sites with n = 112; and Siemens: 7 sites with n = 74) with the following parameters: TR/TE =
96 2000/35 ms; 64 averages; 2, 4 or 5 kHz spectral bandwidth; 2048-4096 data points; acquisition
97 time = 2.13 min; 3×3×3 cm³ voxel in the medial parietal lobe (**Figure 1A**). The water suppres-
98 sion pulse bandwidth was 140 Hz for Philips, 50 Hz for Siemens, and 150 Hz for GE. Reference
99 spectra were acquired with similar parameters, but without water suppression and 8-16 averages.
100 No more acquisition parameters were specified (for more details, please refer to ¹⁷). Data were
101 saved in vendor-native formats (GE P-files, Philips .sdat, and Siemens TWIX). In the initial
102 study¹⁸, written informed consent was obtained from each participant and the study was ap-
103 proved by local institutional review boards. Anonymized data were shared securely and analyzed
104 at Johns Hopkins University with local IRB approval. Due to site-based data privacy guidelines,
105 only a subset of these data (GE: 7 sites with n = 79; Philips: 9 sites with n = 100; and Siemens: 4
106 sites with n = 48) is publicly available¹⁹.

107

108 Data pre-processing

109 MRS data were pre-processed in Osprey⁵, an open-source MATLAB toolbox, following recent
110 peer-reviewed pre-processing recommendations², as summarized in **Figure 1B**. First, the vendor-
111 native raw data were loaded, including the metabolite (water-suppressed) data and unsuppressed
112 water reference data. Second the raw data were pre-processed into averaged spectra. Receiver-
113 coil combination²⁰ and eddy-current correction²¹ of the metabolite data were performed using the
114 water reference data. Individual transients in Siemens and GE data were frequency-and-phase
115 aligned using robust spectral registration²², while Philips data had been averaged on the scanner.
116 After averaging the individual transients, the residual water signal was removed with a Hankel
117 singular value decomposition (HSVD) filter²³. For Siemens spectra, an additional pre-phasing
118 step was introduced by modelling the signals from creatine and choline-containing compounds at
119 3.02 and 3.20 ppm with a double Lorentzian model and applying the inverted model phase to the

120 data. This step corrected a zero-order phase shift in the data arising from the HSVD water re-
121 moval, likely because the Siemens water suppression introduced asymmetry to the residual water
122 signal. Finally, the pre-processed spectra were exported in .RAW format.
123



124

Figure 1. Voxel position and overview of the MRS analysis pipeline. (A) Representative voxel position in the medial parietal lobe extracted with ‘OspreyCoreg’ (B) Pre-processing pipeline implemented in Osprey including ‘OspreyLoad’ to load the vendor-native spectra, ‘OspreyProcess’ to process the raw data and to export the averaged spectra. (C) Modelling of the averaged spectra with details of the basis set and parameters of each LCM (LCModel, Osprey, and Tarquin).

125 Data modelling

126 Fully localized 2D density-matrix simulations implemented in the MATLAB toolbox FID-A²⁴
127 with vendor-specific refocusing pulse information, timings, and phase cycling were used to gen-
128 erate three vendor-specific basis sets (GE, Philips, and Siemens) including 19 spin systems:
129 ascorbate, aspartate, Cr, negative creatine methylene (-CrCH₂), γ -aminobutyric acid (GABA),
130 glycerophosphocholine (GPC), glutathione, glutamine (Gln), glutamate (Glu), water (H₂O), myo-
131 inositol (mI), lactate, NAA, N-acetylaspartylglutamate (NAAG), phosphocholine (PCh), PCr,
132 phosphoethanolamine, scyllo-inositol, and taurine. The -CrCH₂ term is a simulated negative cre-
133 atine methylene singlet at 3.95 ppm, included as a correction term to account for effects of water
134 suppression and relaxation. It is not included in the tCr model, which is used for quantitative ref-
135 erencing.

136 8 additional Gaussian basis functions were included in the basis set to simulate broad macromol-
137 ecules and lipid resonances²⁵ (simulated as defined in section 11.7 of the LCMModel manual²⁶):
138 MM_{0.94}, MM_{1.22}, MM_{1.43}, MM_{1.70}, MM_{2.05}, Lip09, Lip13, Lip20. The Gaussian amplitudes were
139 scaled relative to the 3.02 ppm creatine CH₃ singlet in each basis set (details in **Supplementary**
140 **Material 1**). Finally, to standardize the basis set for each algorithm, basis sets were stored as
141 .mat files for use in Osprey and as .BASIS-files for use in LCMModel and Tarquin. In the follow-
142 ing paragraphs, each LCM algorithm investigated in this study is described briefly (for details,
143 please refer to the original publications^{5,7,11}).

144

145 LCModel v6.3

146 The LCMModel (6.3-0D) algorithm¹¹ models data in the frequency-domain. First, time-domain
147 data and basis functions are zero-filled by a factor of two. Second, frequency-domain spectra are
148 frequency-referenced by cross-correlating them with a set of delta functions representing the ma-
149 jor singlet landmarks of NAA (2.01 ppm), Cr (3.02 ppm), and Cho (3.20 ppm). Third, starting
150 values for phase and linebroadening parameters are estimated by modelling the data with a re-
151 duced basis set containing NAA, Cr, PCh, Glu, and mI, with a smooth baseline. Fourth, the final
152 modelling of the data is performed with the full basis set, regularized lineshape model and base-
153 line, with starting values for phase, linebroadening, and lineshape parameters derived from the
154 previous step. Model parameters are determined with a Levenberg-Marquardt^{27,28} non-linear
155 least-squares optimization implementation that allows bounds to be imposed on the parameters.

156 Metabolite amplitude bounds are defined to be non-negative, and determined using a non-nega-
157 tive linear least-squares (NNLS) fit at each iteration of the non-linear optimization. Amplitude
158 ratio constraints on macromolecule and lipid amplitude, as well as selected pairs of metabolite
159 amplitudes (e.g. NAA+NAAG), are defined as in Osprey and Tarquin. LCMoel constrains the
160 model with three additional regularization terms. Two of these terms penalize a lack of smooth-
161 ness in the baseline and lineshape models using the second derivative operator, preventing unrea-
162 sonable baseline flexibility and lineshape irregularity. The third term penalizes deviations of the
163 metabolite Lorentzian linebroadening and frequency shift parameters from their expected values.
164

165 *Osprey*

166 The Osprey (1.0.0) algorithm⁵ adopts several key features of the LCMoel and Tarquin algo-
167 rithms. Osprey follows the four-step workflow of LCMoel including zero-filling, frequency ref-
168 erencing, preliminary optimization to determine starting values, and final optimization over the
169 real part of the frequency-domain spectrum. The model parameters are zero- and first-order
170 phase correction, global Gaussian linebroadening, individual Lorentzian linebroadening, and in-
171 dividual frequency shifts, which are applied to each basis function before Fourier transformation.
172 The frequency-domain basis functions are then convolved with an arbitrary, unregularized line-
173 shape model to account for deviations from a Voigt profile. The length of this lineshape model is
174 estimated during the initial referencing step and set to 2.5 times the FWHM estimate. The line-
175 shape model is normalized, so that the convolution does not impact the integral of basis func-
176 tions.

177 The spline baseline is constructed from cubic B-spline basis functions, including one additional
178 knot outside either end of the user-specified fit range, as in LCMoel. In contrast to LCMoel,
179 the baseline curvature is not regularized. Therefore, the baseline knot spacing is set to 0.15 ppm
180 for preliminary modelling step with a reduced basis set and increased to 0.4 ppm for the final full
181 model. Similar to LCMoel, model parameters are determined with a Levenberg-Marquardt^{27,28}
182 non-linear least-squares optimization algorithm and a NNLS fit to determine the non-negative
183 metabolite amplitudes at each step of the non-linear optimization.

184 *Tarquin*

185 Tarquin (4.3.10)⁷ uses a four-step approach in the time domain to model spectra. First, residual
186 water is removed using singular value decomposition. Second, the global zero-order phase is

187 determined by minimizing the difference between the magnitude and the real spectra in the fre-
188 quency domain. Third, zero-filling to double the number of points and frequency referencing are
189 performed, as in the other algorithms. This step also estimates a starting value for the Gaussian
190 linebroadening used in the fourth step, the final modelling. The model includes common Gauss-
191 ian linebroadening, individual Lorentzian linebroadening, individual frequency-shifts, and zero-
192 and first-order phase correction factors applied in the frequency domain.
193 Optimization is performed in the time domain with a constrained non-linear least-squares Leven-
194 berg-Marquardt solver, allowing bounds and constraints on the parameters. In addition, the range
195 of time-domain datapoints is limited by removing the first 10 ms of the FID, so as to omit the
196 fast-decaying macromolecule and lipid signals. Finally, the baseline is estimated in the frequency
197 domain by convolving the model residual with a Gaussian filter with a width of 100 points.

198

199 Model parameters

200 The parameters chosen for each tool are summarized in **Figure 1C**. The fit range was limited to
201 0.5 to 4 ppm in all tools to reduce effects of differences in water suppression techniques. For the
202 baseline handling, the default and most commonly used parameters were chosen, i.e. bLine-
203 KnotSpace = 0.4 ppm for Osprey, DKNMNT = 0.15 ppm for LCModel, and an FID range from
204 10 ms to 50% of the FID for Tarquin.

205

206 Quantification, visualization, and secondary analyses

207 Quantification

208 The four major metabolite complexes tNAA (NAA + NAAG), tCho (GPC + PCh), mI, and Glx
209 (Glu + Gln) were quantified as basis-function amplitude ratios relative to total creatine (tCr = Cr
210 + PCr). Since the primary purpose was to compare performance of the core LCM algorithms, no
211 additional relaxation correction or partial volume correction was performed.

212 Model visualizations were generated with the *OspreyOverview* module, which allows LCModel
213 and Tarquin results files (.coord and .txt) to be imported. For each algorithm, the visualization
214 includes site-mean spectra, cohort-mean spectra (i.e. the mean of all spectra), and site- and co-
215 hort-mean modelling results (complete model, spline baseline, spline baseline + MM compo-
216 nents, and the separate models of the major metabolite complexes).

217

218 Visualization

219 As in the default visualizations for the LCModel and Tarquin software interfaces, inverse phase
220 estimates were applied to the spectra and final models. For the visualization, spectra were nor-
221 malized to the amplitude of the 3-ppm creatine singlet, and a DC offset was added to each site
222 mean spectrum to align the mean frequency-domain amplitude between 1.85 and 4.0 ppm, to aid
223 visual comparison between algorithms and sites.

224

225 Secondary analyses

226 To investigate potential vendor differences in linewidth and SNR based on the different export
227 formats of the data, NAA linewidth and SNR were investigated.

228 To investigate potential interactions between baseline power and metabolite estimates unbiased
229 by DC offsets, the MM + baseline models were first aligned vertically according to the fre-
230 quency-domain minimum of the acquired spectra between 2.66 and 2.7 ppm (i.e. between the as-
231 partyl signals, which is the region with the highest consistency between the baseline models).

232 Baseline models were normalized to the frequency-domain amplitude of each metabolite spec-
233 trum between 2.9 and 3.1 ppm to account for differences in the scaling of the model outputs of
234 LCModel and Tarquin. Baseline power beneath each major metabolite was then defined as the
235 range-normalized integral of the baseline model between 1.9 and 2.1 ppm for the tNAA baseline;
236 3.1 and 3.3 ppm for the tCho baseline; 3.33 and 3.75 ppm for mI; and 1.9 to 2.5 ppm and 3.6 to
237 3.8 ppm for the Glx baseline.

238 The contribution of variance in modelling of the creatine reference signal to metabolite ratios
239 was also investigated. To this end, each individual total creatine model (Cr + PCr) was normal-
240 ized to the frequency-domain amplitude of each metabolite spectrum between 1.9 and 2.1 ppm to
241 account for differences in the scaling of the total creatine model outputs of LCModel and Tar-
242 quin. Finally, the integral over the individual creatine model was calculated.

243

244 Data analysis

245 Quantitative metabolite estimates (tNAA/tCr, tCho/tCr, mI/tCr, Glx/tCr) were statistically ana-
246 lyzed and visualized using R²⁹ in RStudio (Version 1.2.5019, RStudio Inc.). The functions are
247 publicly available³⁰. The supplemental materials with MATLAB- and R-files, example LCModel

248 control files (one for each vendor), and Tarquin batch-files for this study are publicly available³¹.
249 The results from each LCM algorithm were imported into R with the *spant* package³².

250

251 Distribution analysis

252 The results are presented as raincloud plots³³ and Pearson's correlation analysis using the
253 *ggplot2* package³⁴. The raincloud plots include individual data points, boxplots with median and
254 25th/75th percentiles, a smoothed distribution, and mean \pm SD error bars to identify systematic
255 differences between the LC algorithms. In addition, the coefficient of variation (CV = SD/mean)
256 and the mean $\overline{CV} = \frac{(CV_{tNAA} + CV_{tCho} + CV_{Ins} + CV_{Glx})}{4}$ across all four metabolites of each algorithm are
257 calculated.

258

259 Correlation analysis

260 The correlation analysis featured different levels, including pair-wise correlations between algo-
261 rithms, as well as correlations between baseline power and metabolite estimates of each algo-
262 rithm. The pair-wise correlation on the global level (black R^2), as well as within-vendor correla-
263 tions (color-coded R^2) with different color shades for different sites are reported. Furthermore,
264 mean $\overline{R^2}$ for each pair-wise correlation (e.g. Osprey vs LCModel) and metabolite, estimated by
265 row or column means e.g. $\overline{R^2} = \frac{(R_{tNAA}^2 + R_{tCho}^2 + R_{Ins}^2 + R_{Glx}^2)}{4}$, and a cohort mean $\overline{R^2}$ (across all pair-
266 wise correlations) are calculated. The correlations were Bonferroni corrected for the number of
267 correlation tests. The cohort mean $\overline{R^2}$ was used to identify global associations across all corre-
268 lation analysis, while the mean $\overline{R^2}$ allowed the identification of algorithm-specific (row means)
269 and metabolite-specific (column means) interactions across all correlation analysis. Associations
270 between the outcome of specific algorithms were identified by the pair-wise correlation analysis
271 (R^2). Vendor-specific effects were identified by differentiating between global level and within-
272 vendor correlations.

273

274 *Statistical analysis*

275 In the statistical analysis, the presence of significant differences in the mean and the variance of
276 the metabolite estimates was assessed. Global metabolite estimates were compared between al-
277 gorithms with parametric tests, following recommendations for large sample sizes³⁵. Differences
278 of variances were tested with Fligner-Killeen's test with a post-hoc pair-wise Fligner-Killeen's
279 test and Bonferroni correction for the number of pair-wise comparisons. Depending on whether
280 variances were different or not, an ANOVA or Welch's ANOVA was used to compare means
281 with a post-hoc paired t-test with equal or non-equal variances, respectively.

282

283

284 **Results**

285 All 277 spectra were successfully processed, exported, and quantified with the three LCM algo-
286 rithms; no modelled spectra were excluded from further analysis.

287 Summary and visual inspection of the modelling results

288 A site-level averaged summary of the 277 spectra is shown in **Figure 2A, B and C**, for analyses
289 in LCModel, Osprey, and Tarquin, respectively. The averaged data, models and residuals for
290 each of the 25 sites are color-coded by vendor. The cohort-mean of all analyses for each vendor
291 is shown in **Figure 2D, E and F** (GE, Philips and Siemens, respectively). Data, models and re-
292 siduals are color-coded by algorithm.

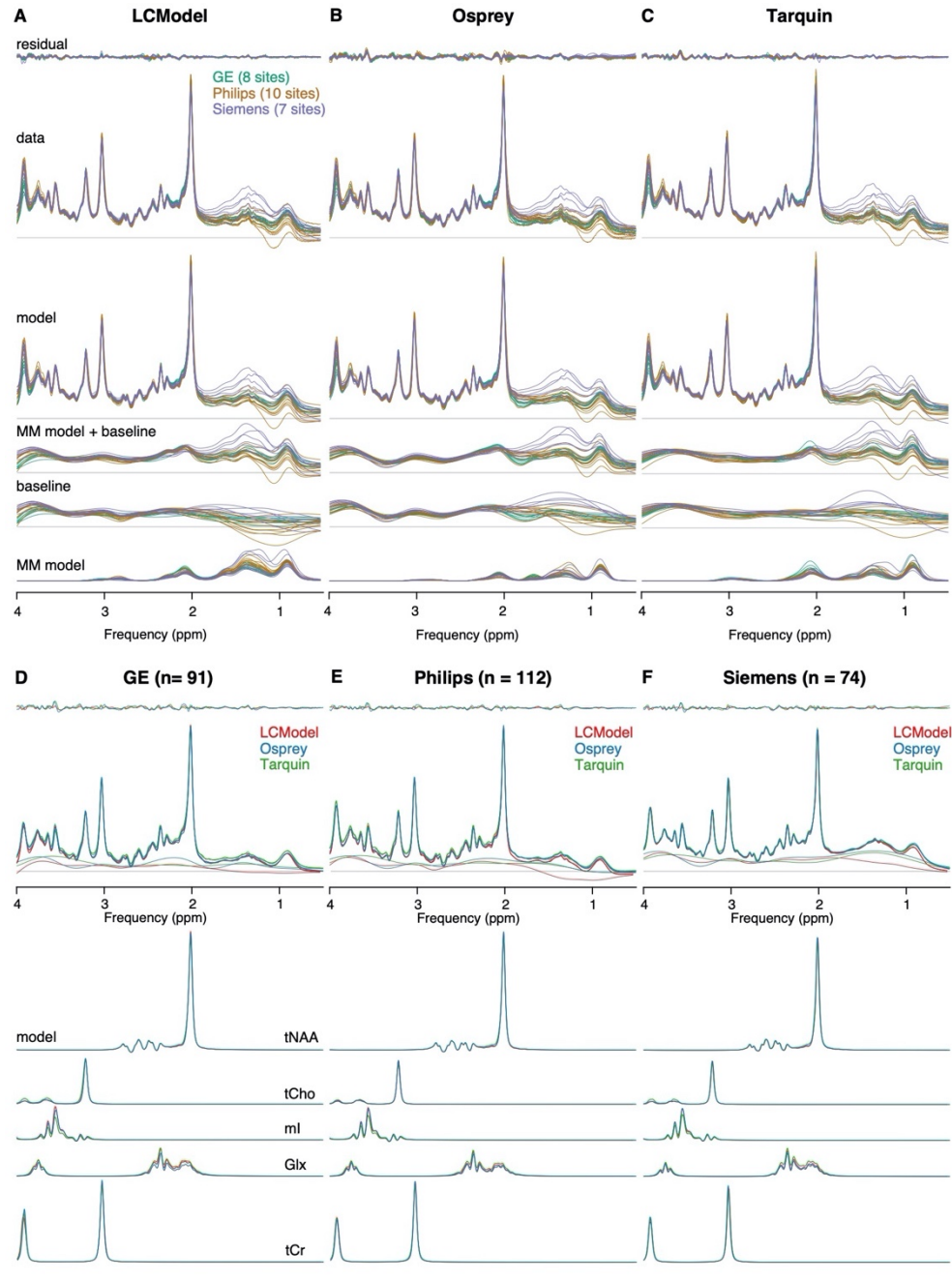
293

294 In general, the phased spectra and models agreed well between vendors for all algorithms. Com-
295 paring the algorithms, notable differences in spectral features in the estimated baseline models
296 appeared between 0.5 and 1.95 ppm (degree of variability: Osprey > LCModel > Tarquin) and
297 between 3.6 and 4 ppm (degree of variability: LCModel > Osprey > Tarquin) (as shown in **Fig-
298 ure 2A-C**).

299 Cohort-mean spectra and models agreed well across all vendors and algorithms (**Figure 2D-F**).
300 The greatest differences in the spectral features of the baseline between algorithms occur be-
301 tween 0.5 and 1.95 ppm, with closer agreement between Osprey and Tarquin than with
302 LCModel. The amplitude of the residual over the whole spectral range is highest for Osprey, and
303 similar for Tarquin and LCModel. **Supplementary Material 2** shows individual data, models
304 and residuals for each algorithm color-coded by vendor.

305 NAA linewidth was significantly lower ($p < 0.001$) for Philips (6.3 ± 1.3 Hz) compared to GE
306 (7.3 ± 1.5 Hz), while no differences in the linewidth were found for the other comparisons (Sie-
307 mens 6.6 ± 2.4 Hz). SNR was significantly higher for Siemens (285 ± 72) compared to both
308 other vendors ($p < 0.001$) and significantly higher ($p < 0.001$) for Philips (226 ± 58) compared to
309 GE (154 ± 37).

310

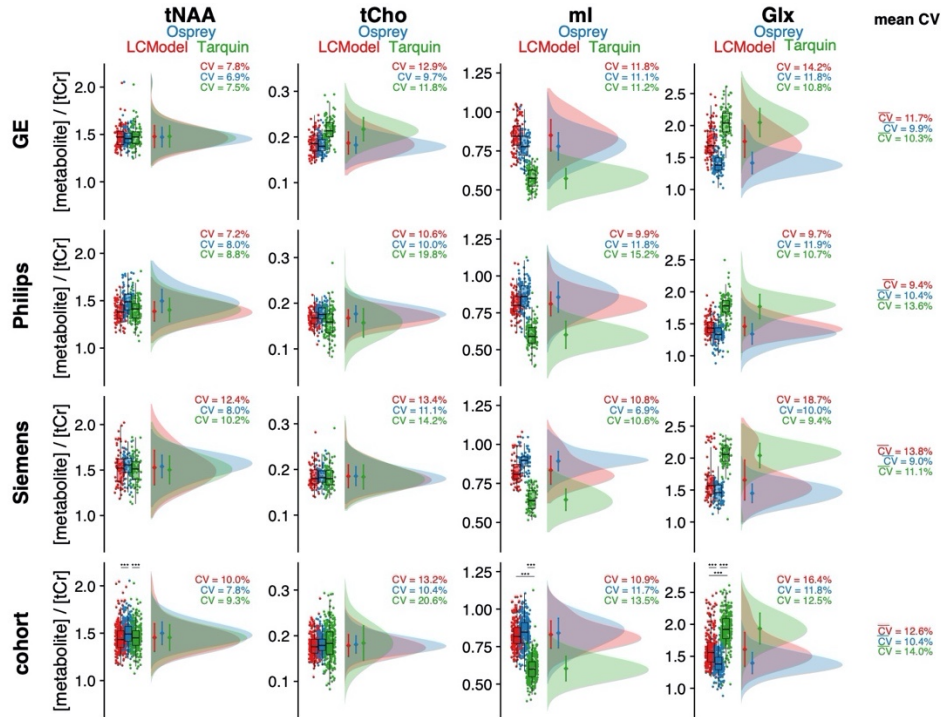


311

Figure 2. Summary of the modelling results. (A–C) site-level averaged residual, data, model, MM model + baseline, baseline and MM model for each LCM algorithm, color-coded by vendor. (D–F) cohort-mean residual, data, model, MM model + baseline, and metabolite models for each vendor, color-coded by LCM algorithm.

312 Metabolite level distribution

313 The tCr ratio estimates and CVs of the four metabolites are summarized in **Table 2**. Distributions
 314 and group statistics are visualized in **Figure 3**, with the four rows corresponding the three ven-
 315 dors and a cohort summary across all datasets.



316

Figure 3. Metabolite level distribution. Raincloud plots of the metabolite estimates of each LCM algorithm (color-coded). The four metabolites are reported in the columns, and the three vendors in rows, with a cohort summary in the last row. The coefficient of variation is reported for each distribution, as well as a mean CV reported in the last column, which is calculated across each row. Asterisks indicate significant differences (adjusted $p < 0.001 = ***$).

317

318 Between-algorithm agreement was greatest for the group means and CVs of tNAA and tCho.

319 The cohort-mean CV was lowest for Osprey (10.4%), followed by LCMModel (12.6%) and Tar-
 320 quin (14.0%). Group means and CVs for tNAA are relatively consistent. As a result, the cohort-
 321 mean tNAA/tCr was 1.45 ± 0.15 for LCMModel, 1.50 ± 0.12 for Osprey, and 1.45 ± 0.14 for Tar-
 322 quin, with significant differences between Osprey and both other LCM algorithms.

323 Cohort means for tCho showed a high agreement between all algorithms. The global CV of tCho
 324 estimates was significantly higher for Tarquin compared to both other algorithms, and

325 significantly lower for Osprey compared to LCModel. Global tCho/tCr was 0.18 ± 0.02 for
 326 LCModel, 0.18 ± 0.02 for Osprey, and 0.18 ± 0.04 for Tarquin.

327 **Table 2** – Metabolite level distribution. Mean, standard deviation and coefficient of variation
 328 (CV) of each metabolite-to-creatine ratio, listed by algorithm and vendor as well as global
 329 summary values. Asterisks indicate significant differences (adjusted $p < 0.01 = **$ and adjusted
 330 $p < 0.001 = ***$ or $####$ or $''''$) in the mean (for the metabolite ratios) or the variance (for the CV)
 331 compared to the algorithm in the next row (LCModel vs Osprey = $**$ or $***$, Osprey vs Tarquin
 332 = $####$, and Tarquin vs LCModel = $''''$).

	[metabolite] / [tCr] (mean \pm SD)			
	tNAA	tCho	mI	Glx
GE				
LCModel	1.48 ± 0.12	0.19 ± 0.02	0.85 ± 0.10	1.75 ± 0.25
Osprey	1.47 ± 0.10	0.18 ± 0.02	0.78 ± 0.09	1.42 ± 0.17
Tarquin	1.48 ± 0.11	0.22 ± 0.03	0.57 ± 0.07	2.05 ± 0.22
Philips				
LCModel	1.38 ± 0.10	0.17 ± 0.02	0.81 ± 0.08	1.46 ± 0.14
Osprey	1.50 ± 0.12	0.18 ± 0.02	0.86 ± 0.10	1.34 ± 0.16
Tarquin	1.40 ± 0.12	0.16 ± 0.03	0.60 ± 0.09	1.78 ± 0.19
Siemens				
LCModel	1.52 ± 0.19	0.19 ± 0.02	0.83 ± 0.09	1.65 ± 0.31
Osprey	1.54 ± 0.12	0.19 ± 0.02	0.89 ± 0.06	1.45 ± 0.14
Tarquin	1.50 ± 0.15	0.18 ± 0.03	0.65 ± 0.07	2.04 ± 0.19
global				
LCModel	$1.45 \pm 0.15^{***}$	0.18 ± 0.02	0.83 ± 0.09	$1.45 \pm 0.15^{***}$
Osprey	$1.50 \pm 0.12^{####}$	0.18 ± 0.02	$0.84 \pm 0.09^{####}$	$1.50 \pm 0.12^{####}$
Tarquin	1.46 ± 0.14	0.18 ± 0.04	$0.60 \pm 0.08^{''''}$	$1.93 \pm 0.24^{''''}$
	CV (SD/mean)			
	tNAA	tCho	mI	Glx
GE				
LCModel	7.9%	12.9%	11.8%	14.2%
Osprey	6.9%	9.7%	11.1%	11.8%
Tarquin	7.5%	11.7%	11.2%	10.8%
Philips				
LCModel	7.2%	10.6%	9.9%	9.7%
Osprey	8.0%	10.0%	11.8%	11.9%
Tarquin	8.8%	19.8%	15.2%	10.7%
Siemens				
LCModel	12.4%	13.4%	10.8%	18.7%
Osprey	8.0%	11.1%	6.9%	10.0%
Tarquin	10.1%	14.3%	10.5%	9.3%
global				
LCModel	10.0%	13.2%**	10.9%	16.4%***
Osprey	7.8%	10.4%####	11.7%####	11.8%####
Tarquin	9.3%	20.5%''''	13.6%	12.3%

333

334

335 For mI, group means and CVs were comparable for Osprey and LCMModel, while Tarquin esti-
336 mates were lower by about 25%. Global CVs were significantly lower for Osprey compared to
337 Tarquin, while no significant differences in the CV were found for the other comparisons. Global
338 mI/tCr was 0.83 ± 0.09 for LCMModel, 0.84 ± 0.09 for Osprey, and 0.60 ± 0.08 for Tarquin, with
339 significant mean differences between all Tarquin and both other algorithms.
340 Group means and CVs for Glx were comparable between Osprey and LCMModel, while estimates
341 were about 30% higher in Tarquin. Global CV was significantly lower for Osprey compared to
342 both other algorithms. Global Glx/tCr was 1.45 ± 0.15 for LCMModel, 1.50 ± 0.12 for Osprey, and
343 1.93 ± 0.24 for Tarquin, with significant differences between all algorithms. Mean \overline{CVs} , esti-
344 mated by the row-mean, were between 9.0 and 13.8% for all algorithms and vendors.

345

346 Correlation analysis: pairwise comparison between LCM algorithms

347 The correlation analysis for each metabolite and algorithm pair is summarized in **Figure 4**. $\overline{R^2}$
348 for each algorithm pair and metabolite are reported in the corresponding row and column, re-
349 spectively.

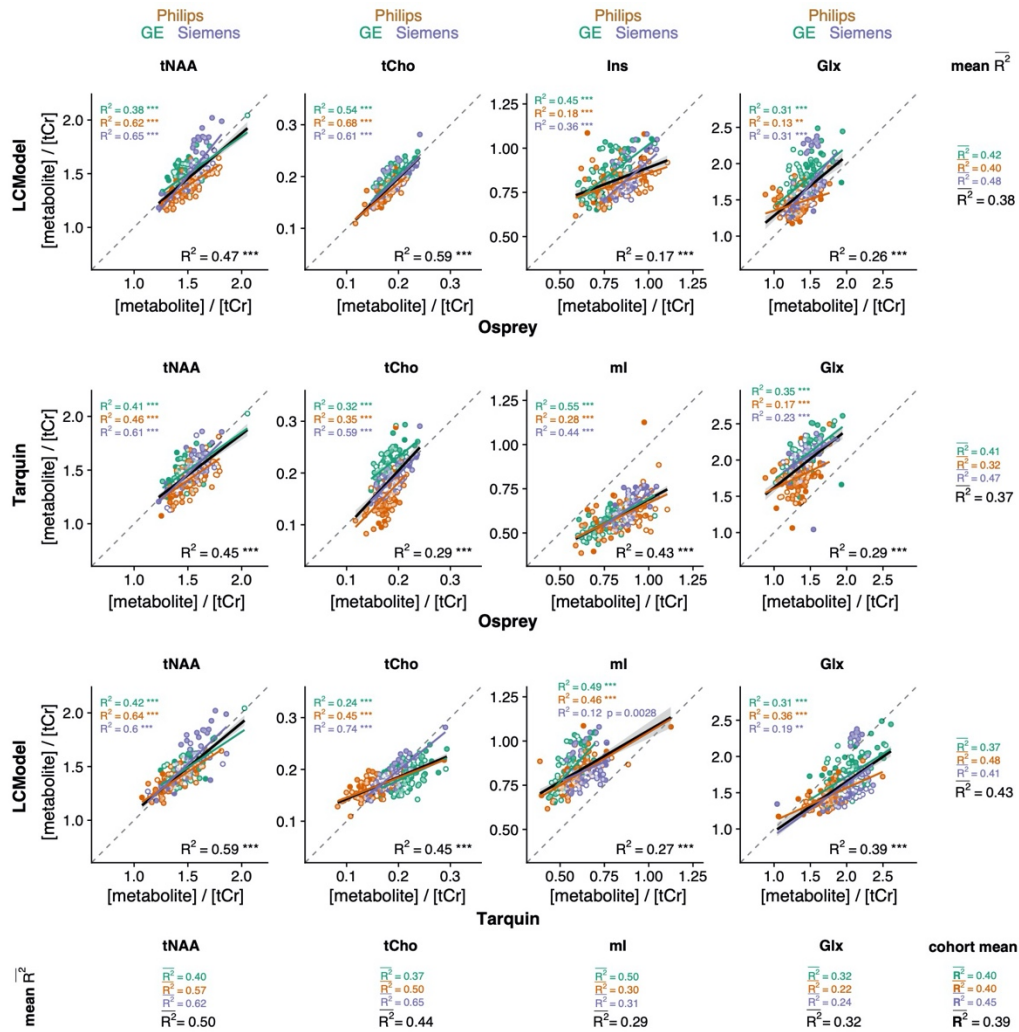
350 The cohort-mean $\overline{R^2} = 0.39$ suggests an overall moderate agreement between metabolite esti-
351 mates from different algorithms. The agreement between algorithms, estimated by the row-mean
352 $\overline{R^2}$, was highest for Tarquin-vs-LCMModel ($\overline{R^2} = 0.43$), followed by Osprey-vs-LCMModel ($\overline{R^2}$
353 $= 0.38$), and Osprey-vs-Tarquin ($\overline{R^2} = 0.37$).

354 The agreement between algorithm for each metabolite, estimated by the column-mean $\overline{R^2}$, was
355 highest for tNAA ($\overline{R^2} = 0.50$), followed by tCho ($\overline{R^2} = 0.44$), Glx ($\overline{R^2} = 0.32$), and mI ($\overline{R^2} =$
356 0.29). The cohort-mean $\overline{R^2}$ for each vendor was higher for Siemens ($\overline{R^2} = 0.45$) than for GE
357 ($\overline{R^2} = 0.40$) and Philips ($\overline{R^2} = 0.40$).

358

359 While the within-metabolite mean $\overline{R^2}$ (average down the columns in Figure 4) are comparable
360 between vendors, there is substantially higher variability of the R^2 values with increasing

361 granularity of the analysis. **Supplementary Material 3** includes an additional layer of correla-
 362 tions at the site level.

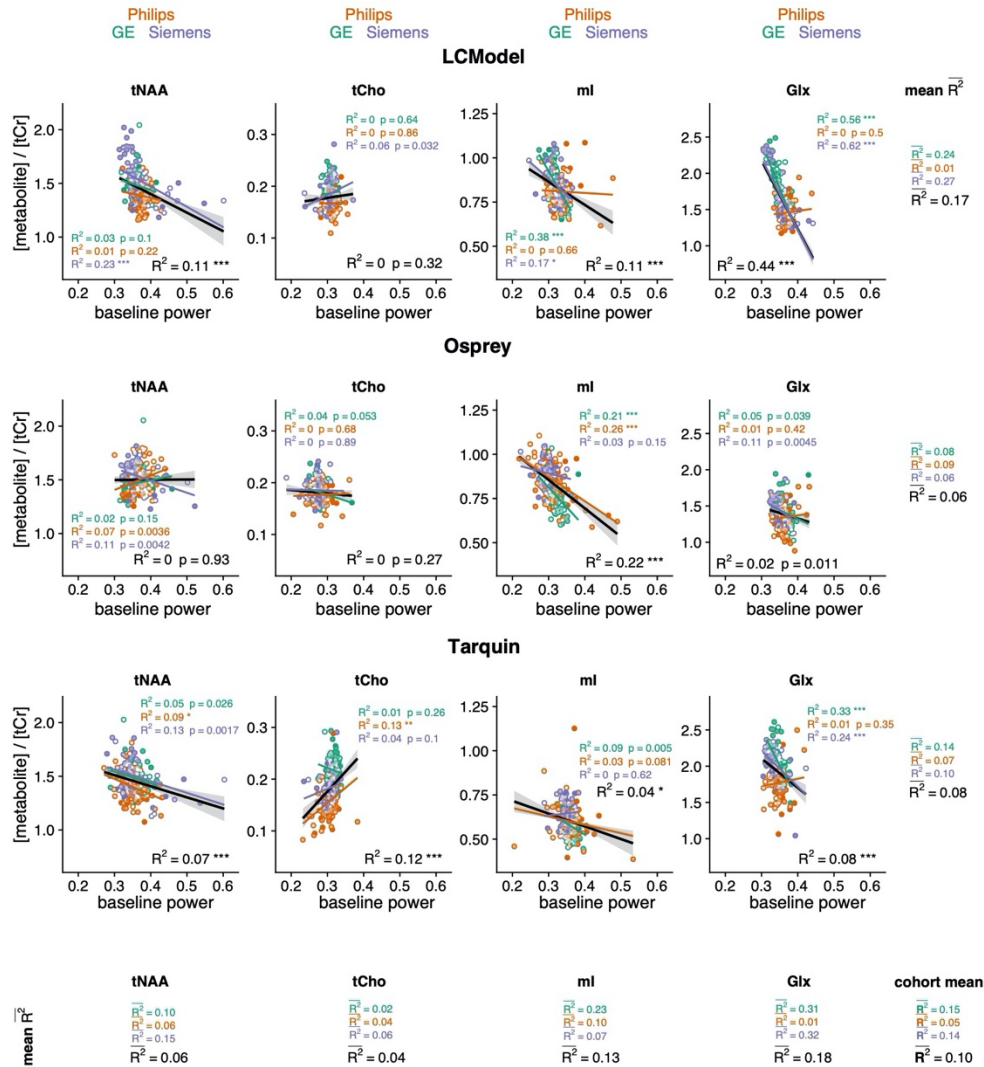


363

364

Figure 4. Pairwise correlational comparison of algorithms. LCMoDel and Osprey are compared in the first row, Tarquin and Osprey in the second row, and LCMoDel and Tarquin in the third row. Each column corresponds to a different metabolite. Within-vendor correlations are color-coded; global correlations are shown in black. The $\overline{R^2}$ values are calculated along each dimension of the grid with mean $\overline{R^2}$ for each metabolite and each correlation. A cohort-mean $\overline{R^2}$ value is also calculated across all twelve pair-wise correlations. Asterisks indicate significant correlations (adjusted $p < 0.01 = **$ and adjusted $p < 0.001 = ***$).

365 Correlation analysis: baseline and metabolite estimates



366

Figure 5. Correlation analysis between metabolite estimates and local baseline power for each algorithm, including global (black) and within-vendor (color-coded) correlations. The mean $\overline{R^2}$ values are calculated along each dimension of the grid for each metabolite and each algorithm. Similarly, a cohort-mean $\overline{R^2}$ value is calculated across all twelve pair-wise correlations. Asterisks indicate significant correlations (adjusted $p < 0.05 = *$, adjusted $p < 0.01 = **$, adjusted $p < 0.001 = ***$).

367

368

369

370

371

The correlation analysis between local baseline power and metabolite estimates for each algorithm is summarized in **Figure 5**. The cohort-mean $\overline{R^2} = 0.10$ suggests that overall, there is an association between local baseline power and metabolite estimates, that is weak but statistically significant. The influence of baseline on metabolite estimates differs between metabolites, as

372 reflected by the column-mean $\overline{R^2}$ which was lowest for tCho ($\overline{R^2} = 0.04$) and tNAA ($\overline{R^2} =$
373 0.06), and higher for mI ($\overline{R^2} = 0.13$) and Glx ($\overline{R^2} = 0.18$). The global baseline correlations all
374 had negative slope, except for tCho estimates of Tarquin.
375 The mean $\overline{R^2}$ across metabolites for each algorithm, calculated as the row mean, were low for
376 all algorithms with LCMoDel ($\overline{R^2} = 0.17$) showing a greater effect than Tarquin ($\overline{R^2} = 0.08$)
377 and Osprey ($\overline{R^2} = 0.06$). Comparing between vendors, the cohort-mean $\overline{R^2}$ was higher for GE
378 ($\overline{R^2} = 0.15$) and Siemens ($\overline{R^2} = 0.14$) than for Philips ($\overline{R^2} = 0.05$) spectra.

379 Variability of total creatine models

380 Mean tCr model spectra (\pm one standard deviation) are summarized in **Figure 6** for each vendor
381 and LCM algorithm, along with distribution plots of the area under the model.

382 The agreement in mean and CV is greatest between Osprey and Tarquin for all vendors, while
383 tCr areas for LCMoDel appear slightly higher. Differences in water suppression are accounted for
384 with the -CrCH₂ correction term, which is not included in the tCr model used for quantitative ref-
385 erencing.

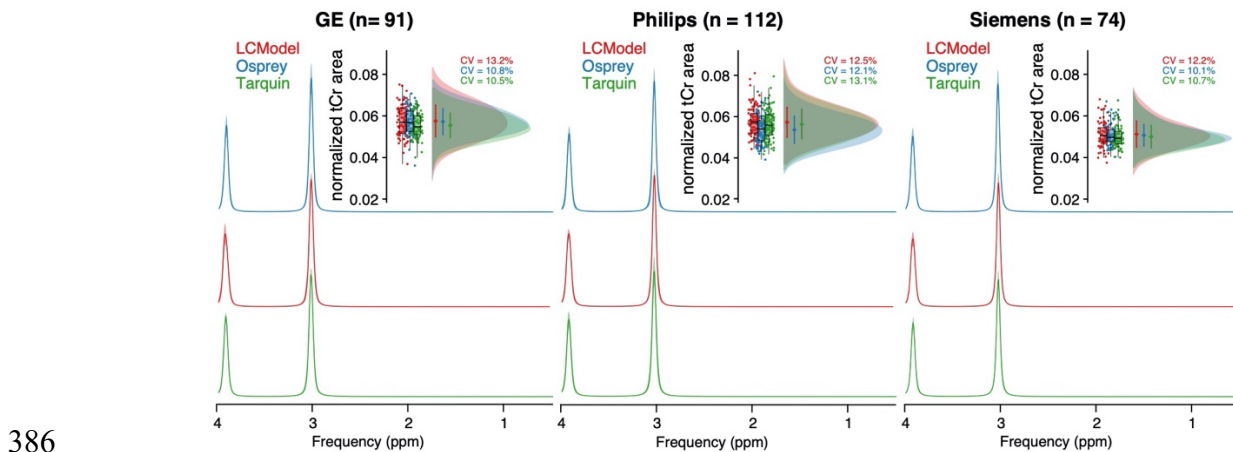


Figure 6. Variability of tCr models. Mean models \pm standard deviation (shaded areas) are presented column-wise by vendor and color-coded by LCM algorithm. The distribution and CV of the areas under the models are inset.

387

388 **Discussion**

389 We have presented a three-way comparison of LCM algorithms applied to a large dataset of
390 short-TE in-vivo human brain spectra. The aims at the onset were to compare metabolite esti-
391 mates obtained with different LCM algorithms, as applied in the literature, and to identify poten-
392 tial sources of differences between the algorithms. The major findings are:

- 393 • Group means and CVs for tNAA and tCho agreed well across vendors and algorithms.
394 For mI and Glx, group means and CVs were less consistent between algorithms, with a
395 higher degree of agreement between Osprey and LCModel than with Tarquin.
- 396 • The strength of the correlations between individual metabolite estimates from different
397 algorithms was moderate. In general, tNAA and tCho estimates from different algorithms
398 agreed better than Glx and mI. With each sub-level of analysis, the variability of
399 correlation strength increased, i.e. correlations grew increasingly variable when
400 calculated separately for each vendor, or even each site.
- 401 • Overall, the association between metabolite estimates and the local baseline power was
402 significant, with mI and Glx showing stronger associations than tNAA and tCho, and
403 LCModel showing greater effects than Tarquin and Osprey.

404 The strong agreement of group means and CVs for metabolites with prominent singlets
405 (tNAA/tCho) and inconsistency for lower-intensity coupled signals (mI/Glx) are in line with pre-
406 vious two-tool comparisons of simulated data ^{7,15} and in-vivo studies with smaller sample sizes
407 ^{7,14,16}.

408 While previous work highlighted group means and standard deviations, the between-algorithm
409 agreement of individual metabolite estimates has not been extensively studied. Our results sug-
410 gest that substantial variability is introduced by the choice of the analysis software itself, indi-
411 cated by only moderate between-algorithm correlation strength (between-algorithm mean $\overline{R^2} \leq$
412 0.5 for all investigated metabolites), even for the well-established LCM algorithms LCModel and
413 Tarquin (R^2 between 0.27 and 0.59 for all metabolites). This finding raises concerns about the
414 generalizability and reproducibility of MRS study results. MRS studies typically suffer from low
415 sample sizes (~20 per comparison group is common). Considering the moderate between-tool
416 correlation of individual estimates, it is likely that marginally significant group effects and corre-
417 lations found with one analysis tool will not be found with another tool, even if the exact same

418 dataset is used. This is exacerbated by the substantial variability of correlation strengths at ven-
419 dor- or even site-level, and is even more likely to be the case for ‘real-life’ clinical data, given
420 the relatively high quality of the dataset in this study (standardized pre-processing; large sample
421 size; high SNR; low linewidth; young, healthy, cooperative subjects). While two previous studies
422 found that some differences between clinical groups remained significant independent of the
423 LCM algorithm^{14,16}, this is questionable as a default assumption. The lack of comparability aris-
424 ing from the additional variability originating in the choice of analysis tool is rarely recognized
425 or acknowledged. If choice of analysis tool is a significant contributor to measurement variance,
426 it could be argued that modelling of data with more than one algorithm will improve the
427 robustness and power of MRS studies. It should also be investigated whether the reduction of the
428 degrees of freedom by improving MM and baseline models (e.g. by using acquired MM data)
429 increases between-tool agreement and consistency between sites and vendors.

430 Sources of variance

431 In order to understand the substantial variability introduced by the choice of analysis tool, the in-
432 fluence of modelling strategies and parameters on quantitative results needs to be better under-
433 stood. Previous investigations have shown that, within a given LCM algorithm, metabolite esti-
434 mates can be affected by the choice of baseline knot spacing^{36,37}, the modelling of MM and lipids
435^{36,38}, and SNR and linewidth³⁹⁻⁴². In this study, we focused on the comparison of each LCM with
436 their default and commonly used parameters, and observed differences resulting both from the
437 default parameters and from differences in the core algorithm. Minor differences in spectral qual-
438 ity (SNR and LW) were found between vendors. The agreement between vendors was high for
439 the mean metabolite levels and the cohort-mean correlations. Further vendor-specific effects on
440 the LCM estimation of this dataset are described elsewhere¹⁷.

441 LCM relies on the assumption that broad background and baseline signals can be separated from
442 narrower metabolite signals. This is true to a limited degree, and the choice of MM and baseline
443 modelling influences the quantification of metabolite resonances⁴. Our secondary analysis of the
444 relationship between baseline power and metabolite estimates showed a stronger interaction for
445 the broader coupled signals of Glx and mI than the singlets. tCho showed the weakest effect, and
446 the three LCMs showed the highest agreement between the MM+baseline models around 3.2
447 ppm. The higher variance of Glx and mI estimates may at least partly be explained by the ab-
448 sence of MM basis functions for frequencies >3 ppm in the model. MM signal must therefore

449 either be modelled by metabolite basis functions or the spline baseline. Including experimental
450 MM acquisitions into studies may reduce the degrees of freedom of modelling, but introduce
451 other sources of variance, such as age-dependency⁴³ or tissue composition^{38,44}. While consensus
452 is emerging that such approaches are recommended many open questions must be resolved be-
453 fore the recommendations can be broadly implemented²⁵.

454 For all three LCM algorithms, optimization between the model and the data is solved by local
455 optimization. Algorithms could converge on a local minimum, if the search space of the non-
456 linear parameters is of high dimensionality, or if the starting values of the parameters are far
457 away from the global optimum⁴⁵. The availability of open-source LCM such as Tarquin and Os-
458 prey will allow further investigation of the relationship between optimization starting values and
459 modelling outcomes.

460

461 Since this study focused on reporting tCr ratios, it is important to consider the variance of the
462 creatine model of each algorithm. With MRS only quantitative in a relative sense, separating the
463 variance contribution of the reference signal is a challenge. While mean tCr model areas were
464 slightly higher for LCModel than for Osprey and Tarquin, there was no generalizable observa-
465 tion of lower tCr ratios from LCModel. CVs of the tCr model areas were comparable across
466 LCM algorithms for each vendor. Vendor differences in water suppression of each vendor were
467 accounted for by limiting the analysis range to 0.5 to 4 ppm, and by including a -CrCH₂ correc-
468 tion term (omitted from calculations of the tCr ratios and the secondary analysis of the tCr mod-
469 els). The contribution of the reference signal to the variance of metabolite estimates is unclear
470 and hard to isolate. Nevertheless, tCr referencing was preferred in this study, since water refer-
471 encing is likely to add additional tool-specific variance resulting from water amplitude estima-
472 tion.

473

474 Limitations

475 As mentioned in greater detail above, there is currently no widely adopted consensus on the defi-
476 nition of MM basis functions, and measured MM background data are not widely available to
477 non-expert users. To reflect common practice in current MRS applications, the default MM basis
478 function definitions from LCModel were adapted for each algorithm in this study. These basis
479 functions only included MMs for frequencies < 3.0 ppm, which is likely insufficient for the

480 modelling of MM signals between 3 and 4 ppm⁴⁶, and will have repercussions for the estimation
481 of tCho, mI, and Glx. Second, standard modelling parameters were chosen for each LCM, which
482 ensure a broader comparability to the current literature, but may not be ideal. Third, there is ob-
483 viously no ‘gold standard’ of metabolite level estimation to validate MRS results against. The
484 performance of an algorithm is often judged based on the level of variance, but low variance
485 clearly does not reflect accuracy and may indicate insufficient responsiveness of a model to the
486 data. In comparing multiple algorithms, it is tempting to infer algorithms that show a higher de-
487 gree of correlation in results are more reliable, but it could equally be the case that shared algo-
488 rithm-based sources of variance increase such correlations. Efforts to use simulated spectra as a
489 gold-standard, including those applying machine learning^{47,48}, can only be successful to the ex-
490 tent that simulated data are truly representative of in-vivo data. Fourth, another criterion to judge
491 the performance of an algorithm is the residual. For example, a small residual indicates a higher
492 agreement between the complete model and the data for LCModel, it does not infer a better esti-
493 mation of individual metabolites, and may result from the higher degree of freedom in the base-
494 line of LCModel (higher number of splines) compared to Osprey and Tarquin. This is empha-
495 sized by the high agreement of the mean mI models, but lower agreement of the baseline models
496 around 3.58 ppm between LCModel and Osprey. Fifth, this study was limited to the two most
497 widely used algorithms LCModel and Tarquin, as well as the Osprey algorithm that is under on-
498 going development in our group. While including additional algorithms would increase the gen-
499 eral understanding of different algorithms, the complexity of the resulting analysis and interpre-
500 tation would be overwhelming and beyond the scope of a single publication.

501

502 **Conclusion**

503 This study presents a comparison of three LCM algorithms applied to a large short-TE PRESS
504 dataset. While different LCM algorithms' estimates of major metabolite levels agree broadly at a
505 group level, correlations between results are only weak-to-moderate, despite standardized pre-
506 processing, a large sample of young, healthy and cooperative subjects, and high spectral quality.
507 The variability of metabolite estimates that is introduced by the choice of analysis software is
508 substantial, raising concerns about the robustness of MRS research findings, which typically use
509 a single algorithm to draw inferences from much smaller sample sizes.

510

511 **Acknowledgement**

512 This work is supported by NIH grants R01 EB016089 R01 EB023963 R21A G060245. GO re-
513 ceives support from NIH grant K99 AG062230. MP is supported by NIH grants P41EB015909
514 and R01NS106292.
515

516 References

- 517 1. Öz G, Alger JR, Barker PB, et al. Clinical Proton MR Spectroscopy in Central Nervous
518 System Disorders. *Radiology*. 2014;270(3):658-679. doi:10.1148/radiol.13130531
- 519 2. Wilson M, Andronesi O, Barker PB, et al. Methodological consensus on clinical proton
520 MRS of the brain: Review and recommendations. *Magn Reson Med*. 2019;82(2):527–550.
521 doi:10.1002/mrm.27742
- 522 3. Bottomley P. *Selective Volume Method for Performing Localized NMR Spectroscopy*. Vol
523 3.; 1985. doi:10.1016/0730-725X(85)90032-3
- 524 4. Near J, Harris AD, Juchem C, et al. Preprocessing, analysis and quantification in single-
525 voxel magnetic resonance spectroscopy: experts' consensus recommendations. *NMR Bio-*
526 *med*. 2020;n/a(n/a):e4257. doi:10.1002/nbm.4257
- 527 5. Oeltzschner G, Zöllner HJ, Hui SCN, et al. Osprey: Open-source processing, reconstruction
528 & estimation of magnetic resonance spectroscopy data. *J Neurosci Methods*.
529 2020;343:108827. doi:10.1016/j.jneumeth.2020.108827
- 530 6. Juchem C. INSPECTOR - A Tool for Teaching Magnetic Resonance Spectroscopy. In: *26th*
531 *Annual Meeting of the International Society for Magnetic Resonance in Medicine (ISMRM)*.
532 Paris, France; 2018.
- 533 7. Wilson M, Reynolds G, Kauppinen RA, Arvanitis TN, Peet AC. A constrained least-
534 squares approach to the automated quantitation of in vivo 1 H magnetic resonance spectros-
535 copy data. *Magn Reson Med*. 2011;65(1):1–12. doi:10.1002/mrm.22579
- 536 8. Pouillet J-B, Sima DM, Simonetti AW, et al. An automated quantitation of short echo time
537 MRS spectra in an open source software environment: AQSES. *NMR Biomed*.
538 2007;20(5):493–504. doi:10.1002/nbm.1112
- 539 9. Soher BJ, Semanchuk P, Todd D, Steinberg J, Young K. VeSPA: Integrated applications
540 for RF pulse design, spectral simulation and MRS data analysis. In: *19th Annual Meeting of*
541 *the International Society for Magnetic Resonance in Medicine (ISMRM)*. Montreal, Canada;
542 2011. <https://cds.ismrm.org/protected/11MProceedings/files/1410.pdf>. Accessed May 19,
543 2020.
- 544 10. Graveron-Demilly D. Quantification in magnetic resonance spectroscopy based on semi-
545 parametric approaches. *Magn Reson Mater Phys Biol Med*. 2014;27(2):113-130.
546 doi:10.1007/s10334-013-0393-4
- 547 11. Provencher SW. Estimation of metabolite concentrations from localized in vivo proton
548 NMR spectra. *Magn Reson Med*. 1993;30(6):672–679. doi:10.1002/mrm.1910300604
- 549 12. Osorio-Garcia MI, Sima DM, Nielsen FU, Himmelreich U, Huffel SV. Quantification of
550 magnetic resonance spectroscopy signals with lineshape estimation. *J Chemom*.
551 2011;25(4):183-192. doi:10.1002/cem.1353

- 552 13. Shen ZW, Chen YW, Wang HY, et al. Quantification of Metabolites in Swine Brain by ¹H
553 MR Spectroscopy Using LCModel and QUEST: A Comparison Study. In: *2008 Congress*
554 *on Image and Signal Processing*. Vol 5. ; 2008:299-302. doi:10.1109/CISP.2008.478
- 555 14. Kossowski B, Orzeł J, Bogorodzki P, Wilson M, Setkowicz Z, P. Gazdzinski S. Follow-up
556 analyses on the effects of long-term use of high fat diet on hippocampal metabolite concen-
557 trations in Wistar rats: Comparing Tarquin quantification of 7.0T rat metabolites to
558 LCModel. *Biol Eng Med*. 2017;2(4). doi:10.15761/BEM.1000129
- 559 15. Mosconi E, Sima DM, Garcia MIO, et al. Different quantification algorithms may lead to
560 different results: a comparison using proton MRS lipid signals. *NMR Biomed*.
561 2014;27(4):431-443. doi:10.1002/nbm.3079
- 562 16. Scott J, Underwood J, Garvey LJ, Mora-Peris B, Winston A. A comparison of two post-pro-
563 cessing analysis methods to quantify cerebral metabolites measured via proton magnetic
564 resonance spectroscopy in HIV disease. *Br J Radiol*. 2016;89(1060):20150979.
565 doi:10.1259/bjr.20150979
- 566 17. Považan M, Mikkelsen M, Berrington A, et al. Comparison of Multivendor Single-Voxel
567 MR Spectroscopy Data Acquired in Healthy Brain at 26 Sites. *Radiology*.
568 2020;295(1):191037. doi:10.1148/radiol.2020191037
- 569 18. Mikkelsen M, Barker PB, Bhattacharyya PK, et al. Big GABA: Edited MR spectroscopy at
570 24 research sites. *NeuroImage*. 2017;159:32–45. doi:10.1016/j.neuroimage.2017.07.021
- 571 19. Big GABA repository. Big GABA repository. https://www.nitrc.org/projects/big_gaba/. Pub-
572 lished 2018. Accessed May 27, 2020.
- 573 20. Hall EL, Stephenson MC, Price D, Morris PG. Methodology for improved detection of low
574 concentration metabolites in MRS: Optimised combination of signals from multi-element
575 coil arrays. *NeuroImage*. 2014;86:35-42. doi:10.1016/j.neuroimage.2013.04.077
- 576 21. Klose U. In vivo proton spectroscopy in presence of eddy currents. *Magn Reson Med*.
577 1990;14(1):26–30. doi:10.1002/mrm.1910140104
- 578 22. Mikkelsen M, Tapper S, Near J, Mostofsky SH, Puts NAJ, Edden RAE. Correcting fre-
579 quency and phase offsets in MRS data using robust spectral registration. *NMR Biomed*. July
580 2020:e4368. doi:10.1002/nbm.4368
- 581 23. Barkhuijsen H, de Beer R, van Ormondt D. Improved algorithm for noniterative time-do-
582 main model fitting to exponentially damped magnetic resonance signals. *J Magn Reson*
583 *1969*. 1987;73(3):553–557. doi:10.1016/0022-2364(87)90023-0
- 584 24. Simpson R, Devenyi GA, Jezzard P, Hennessy TJ, Near J. Advanced processing and simu-
585 lation of MRS data using the FID appliance (FID-A)—An open source, MATLAB-based
586 toolkit. *Magn Reson Med*. 2017;77(1):23–33. doi:10.1002/mrm.26091

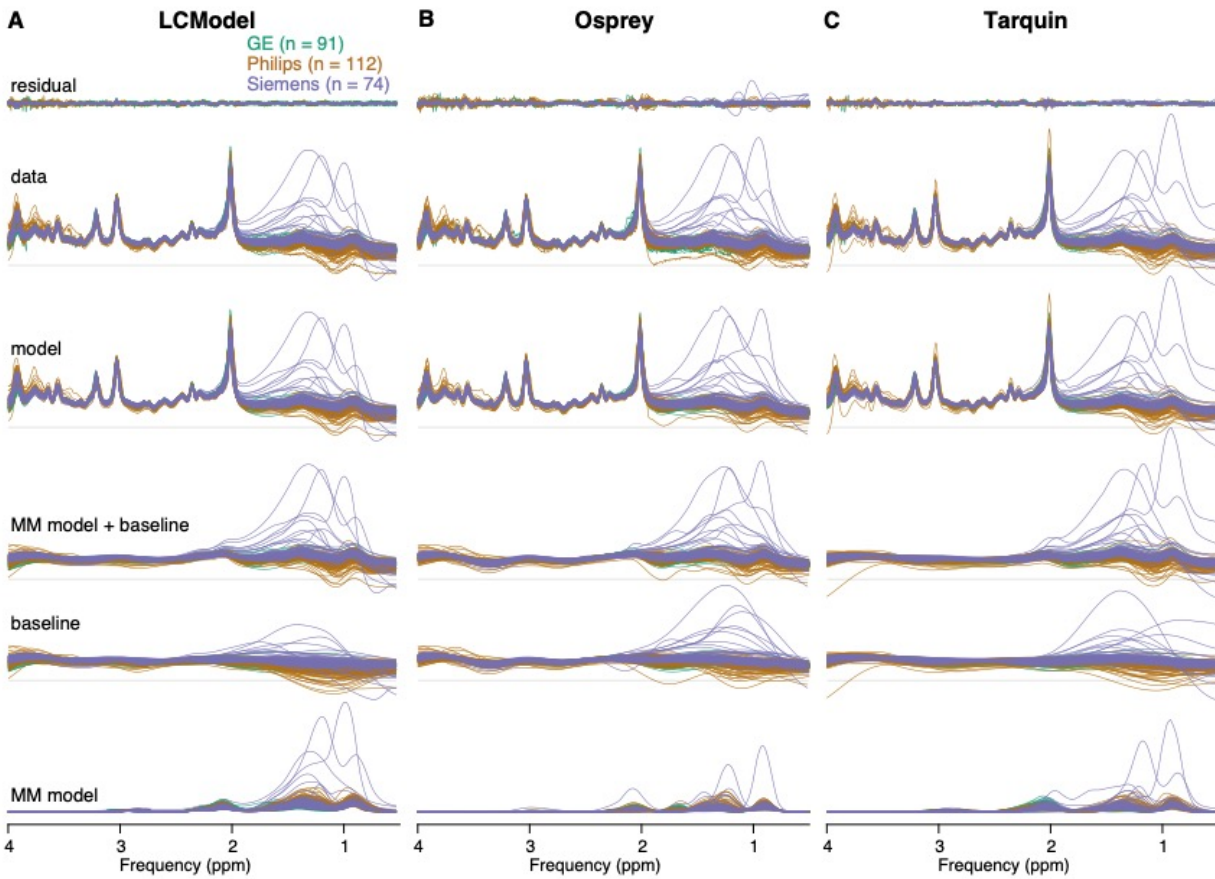
- 587 25. Cudalbu C, Behar KL, Bhattacharyya PK, et al. Contribution of macromolecules to brain
588 1H MR spectra: Experts' consensus recommendations. *NMR Biomed Revis.* 2020.
- 589 26. Provencher S. LCMModel & LCMgui User's Manual. LCMModel & LCMgui User's Manual.
590 <http://s-provencher.com/pub/LCMModel/manual/manual.pdf>. Published 2020. Accessed July
591 15, 2020.
- 592 27. Levenberg K. A method for the solution of certain non-linear problems in least squares. *Q*
593 *Appl Math.* 1944;2(2):164-168. doi:10.1090/qam/10666
- 594 28. Marquardt DW. An Algorithm for Least-Squares Estimation of Nonlinear Parameters. *J Soc*
595 *Ind Appl Math.* 1963;11(2):431-441. doi:10.1137/0111030
- 596 29. R Core Team. *R: A Language and Environment for Statistical Computing.* Vienna, Austria:
597 R Foundation for Statistical Computing; 2017. <https://www.R-project.org/>.
- 598 30. SpecVis GitHub repository. SpecVis GitHub repository.
599 <https://github.com/hezoe100/SpecVis>. Published 2020. Accessed May 27, 2020.
- 600 31. Zöllner HJ. Comparison of algorithms for linear-combination modelling of short-echo-time
601 magnetic resonance spectra. <https://osf.io/3ekq4/>. Published June 1, 2020. Accessed June 2,
602 2020.
- 603 32. <https://github.com/martin3141/spant>. spant GitHub repository. [https://github.com/mar-](https://github.com/martin3141/spant)
604 [tin3141/spant](https://github.com/martin3141/spant). Published 2017. Accessed May 27, 2020.
- 605 33. Allen M, Poggiali D, Whitaker K, Marshall TR, Kievit RA. Raincloud plots: a multi-plat-
606 form tool for robust data visualization. *Wellcome Open Res.* 2019;4:63. doi:10.12688/well-
607 comeopenres.15191.1
- 608 34. Wickham H. *Ggplot2: Elegant Graphics for Data Analysis.* Springer-Verlag New York;
609 2009. <http://ggplot2.org>.
- 610 35. Fagerland MW. T-tests, non-parametric tests, and large studiesa paradox of statistical prac-
611 tice? *BMC Med Res Methodol.* 2012;12(1):78. doi:10.1186/1471-2288-12-78
- 612 36. Marjańska M, Terpstra M. Influence of fitting approaches in LCMModel on MRS quantifica-
613 tion focusing on age-specific macromolecules and the spline baseline. *NMR Biomed.* No-
614 vember 2019. doi:10.1002/nbm.4197
- 615 37. Wenger KJ, Hattingen E, Harter PN, et al. Fitting algorithms and baseline correction influ-
616 ence the results of non-invasive in vivo quantitation of 2-hydroxyglutarate with 1H-MRS.
617 *NMR Biomed.* 2019;32(1):e4027. doi:10.1002/nbm.4027
- 618 38. Schaller B, Xin L, Gruetter R. Is the macromolecule signal tissue-specific in healthy human
619 brain? A ¹H MRS study at 7 tesla in the oc-
620 cipital lobe. *Magn Reson Med.* 2014;72(4):934–940. doi:10.1002/mrm.24995

- 621 39. Bartha R. The Effect of Signal to Noise Ratio and Linewidth On 4T Short Echo Time 1H
622 MRS Metabolite Quantification. *Proc 13th Sci Meet Int Soc Magn Reson Med.*
623 2005;216(1):2459–2459.
- 624 40. Near J. Investigating the effect of spectral linewidth on metabolite measurement bias in
625 short-TE MRS. In: *21th Annual Meeting of the International Society for Magnetic Reso-*
626 *nance in Medicine (ISMRM).* Milan, Italy; 2014.
- 627 41. Wijtenburg SA, Knight-Scott J. The Impact of SNR on the Reliability of LCModel and
628 QUEST Quantitation in 1 H-MRS. In: *17th Annual Meeting of the International Society for*
629 *Magnetic Resonance in Medicine (ISMRM).* ; 2009.
- 630 42. Zhang Y, Shen J. Effects of noise and linewidth on in vivo analysis of glutamate at 3 T. *J*
631 *Magn Reson.* 2020;314. doi:10.1016/j.jmr.2020.106732
- 632 43. Marjańska M, Deelchand DK, Hodges JS, et al. Altered macromolecular pattern and con-
633 tent in the aging human brain. *NMR Biomed.* 2018;31(2):e3865. doi:10.1002/nbm.3865
- 634 44. Považan M, Strasser B, Hangel G, et al. Simultaneous mapping of metabolites and individ-
635 ual macromolecular components via ultra-short acquisition delay 1H MRSI in the brain at
636 7T. *Magn Reson Med.* 2018;79(3):1231-1240. doi:10.1002/mrm.26778
- 637 45. Pouillet J-B, Sima DM, Van Huffel S. MRS signal quantitation: A review of time- and fre-
638 quency-domain methods. *J Magn Reson.* 2008;195(2):134-144.
639 doi:10.1016/j.jmr.2008.09.005
- 640 46. Giapitzakis I-A, Avdievich N, Henning A. Characterization of macromolecular baseline of
641 human brain using metabolite cycled semi-LASER at 9.4T. *Magn Reson Med.*
642 2018;80(2):462-473. doi:10.1002/mrm.27070
- 643 47. Lee HH, Kim H. Deep learning-based target metabolite isolation and big data-driven meas-
644 urement uncertainty estimation in proton magnetic resonance spectroscopy of the brain.
645 *Magn Reson Med.* 2020;n/a(n/a). doi:10.1002/mrm.28234
- 646 48. Lee HH, Kim H. Intact metabolite spectrum mining by deep learning in proton magnetic
647 resonance spectroscopy of the brain. *Magn Reson Med.* 2019;82(1):33-48.
648 doi:10.1002/mrm.27727
- 649

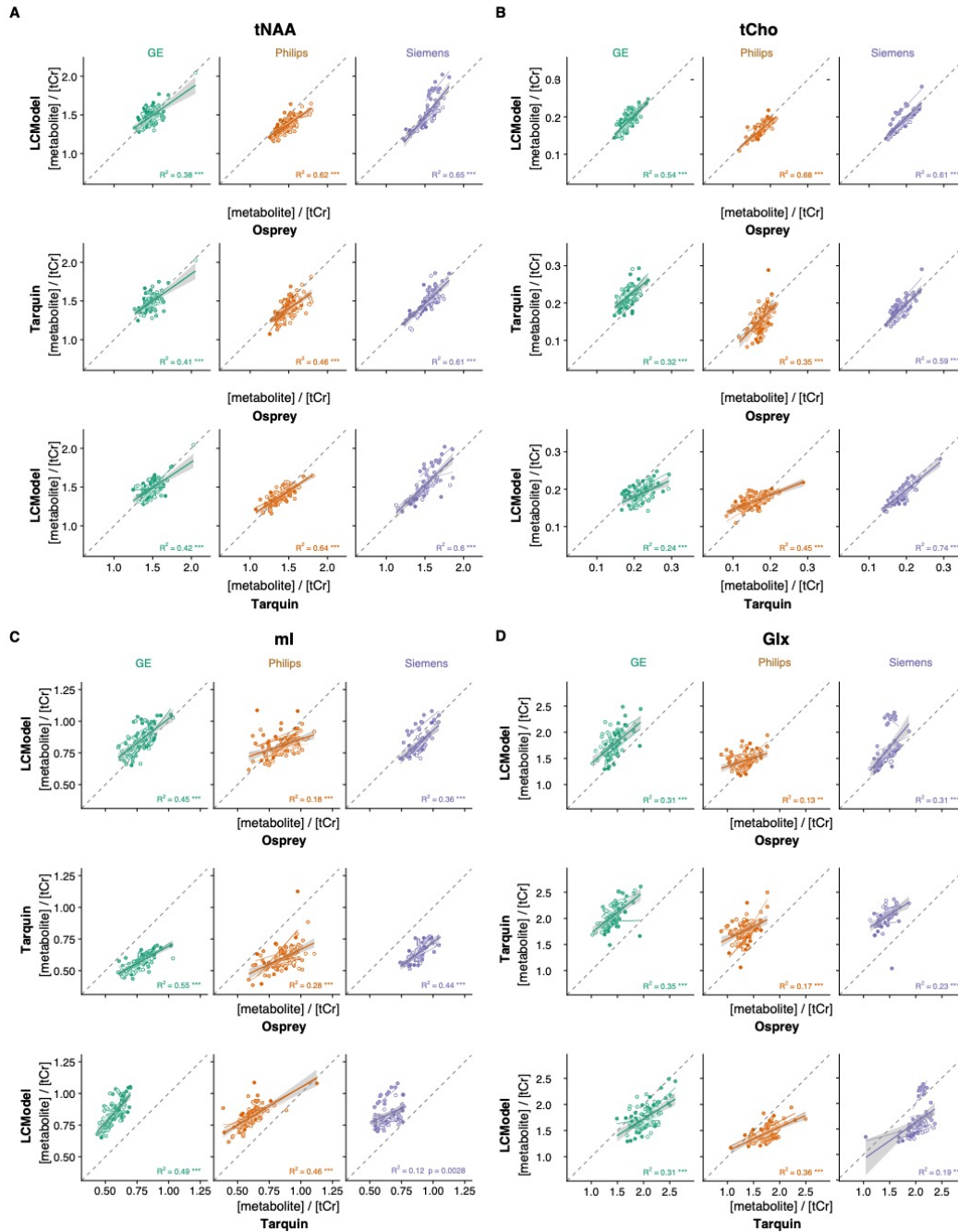
Supplementary Material

<i>Name</i>	<i>Frequencies [ppm]</i>	<i>FWHM [ppm]</i>	<i>Amplitude</i>
MM09	0.91	0.14	3.00
MM12	1.21	0.15	2.00
MM14	1.43	0.17	2.00
MM17	1.67	0.15	0.20
MM20	2.08	0.15	1.33
	2.25	0.20	0.33
	1.95	0.15	0.33
	3.00	0.20	0.40
Lip09	0.89	0.14	3.00
Lip13a	1.28	0.15	2.00
Lip13b	1.28	0.089	2.00
Lip20	2.04	0.15	1.33
	2.25	0.15	0.67
	2.80	0.20	0.87

Supplementary Material 1. *Properties of the Gaussian functions of the broad macromolecule and lipid resonances included in the basis sets, taken from section 11.7 of the LCMoDel manual. The amplitude values are scaled relative to the CH₃ singlet of creatine with amplitude 3.*



Supplementary Material 2. Summary of the individual modelling results. (A–C) individual residuals, data, models, MM models + baseline, baseline and MM models for each LCM algorithm, color-coded by vendor.



Supplementary Material 3. Faceted pair-wise correlational comparison of algorithms. LCMoDel and Osprey are compared in the first row, Tarquin and Osprey are compared in the second row, and LCMoDel and Tarquin are compared in the third row. Each sub-plot (A-D) corresponds to a different metabolite. Within-vendor (bold line with confidence interval) and within-site (thin line) correlations are color-coded. Asterisks indicate significant correlations (adjusted $p < 0.01 = **$ and adjusted $p < 0.001 = ***$).